# Observation of current strings in $Bi_2Sr_2CaCu_2O_8$ single crystals

M. V. Indenbom,* Th. Schuster, H. Kuhn, and H. Kronmüller
*Max-Planck-Institut für Metallforschung, Institut für Physik, 70506 Stuttgart, Germany*

T. W. Li
*Kammerlingh Onnes Laboratorium, Rijksuniversiteit Leiden, P.O. Box 9506, 2300 RA Leiden, The Netherlands*

A. A. Menovsky
*Van der Waals-Zeeman Laboratorium, Universiteit van Amsterdam, Valckenierstraat 65, 1018 XE Amsterdam, The Netherlands*

(Received 1 November 1994)

A flux step between regions of magnetic flux of opposite polarities in the remanent state of $Bi_2Sr_2CaCu_2O_8$ single crystals is observed by means of a high resolution magneto-optical technique. This step indicates a current string inside the crystal platelet which is similar to the string appearing in the solution of the critical state problem for a cylindrical type-II superconducting wire with transport current if one takes into account the finite lower critical field $H_{c1}$. The conditions for the existence of the current string and its properties are discussed.

## I. INTRODUCTION

The classical Bean model[1] which assumes the lower critical field $H_{c1}$ to be zero is often used to describe the magnetic behavior of type-II superconductors; see, e.g., Refs. 2 and 3. In order to find a better description of magnetization curves the critical current density $j_c$ = const in the original Bean model was replaced by a field-dependent critical current density $j_c(B)$.[4] Such a dependence causes the flux-density profiles in an infinitely long cylinder to deviate from the linear slope predicted by the Bean model and to become steeper at the penetrating flux front. A similar effect results when the flux penetration is due to a finite lower critical field $H_{c1}$. The jump of $B(H)$ at the applied field $H = H_{c1}$ causes a vertical slope of $B(\mathbf{r})$ at the flux front which means strong surfacelike supercurrents *inside* the specimen. The additional supercurrent at the flux front can enhance the magnetic moment considerably and in general will change the magnetization curve.[5–7] Since the effect of the additional magnetic moment of the surfacelike current can hardly be resolved by integral magnetization measurements, we performed space-resolved observations of the flux distribution in low-$T_c$ and high-$T_c$ superconductors (HTSC's) using magneto-optical techniques.[8–13]

A sharp boundary between regions of flux with opposite polarities in $YBa_2Cu_3O_7$ (YBCO) single crystals due to finite $H_{c1}$ was recently observed by the high-resolution Faraday technique.[14] The observed flux steps in the flux-density profiles occur only in a temperature range where $H_{c1} \approx j_c d$ ($d$ = sample thickness). In different YBCO single crystals these conditions occur at different temperatures near $T_c$ where the motion of the flux step is irregular. Because of this irregular behavior of the flux steps, it was argued that their occurrence is not a general phenomenon in type-II superconductors.

To clarify this question, we studied the magnetic flux distribution in $Bi_2Sr_2CaCu_2O_{8+\delta}$ (Bi2212) single crystals. Here, the flux steps occur at lower temperatures $T \approx 20$ K where the flux motion is regular. The observation of flux steps in different materials proves their universality.

To explain the observed data we develop a model of the critical state with finite $H_{c1}$ which leads to the appearance of an additional supercurrent localized in a narrow string inside the homogeneous current flow of the critical value $j_c$. However, the flux steps described above cannot be observed when the superconducting films are too thin; this was proved on a YBCO thin film. The reasons for the absence of current strings in thin superconductors will be explained.

## II. EXPERIMENTAL TECHNIQUE

### A. Sample preparation

The Bi2212 single crystals investigated in this paper were grown by the traveling solvent floating zone method as described in Ref. 15. The composition of the crystals was determined by electron probe microanalysis to $Bi_{2.16}Sr_{1.91}Ca_{1.03}Cu_2O_{8+x}$ and from ac susceptibility measurements the superconducting critical temperature was determined to $T_c = 88$ K with a transition width of $\Delta T_c = 2.2$ K. For our investigations we used nearly rectangular crystals with a typical size of $1200 \times 2500 \times 40\ \mu m^3$. The Bi2212 single crystals did not exhibit any macroscopical weak links at $T = 5$ K, which was proved by magneto-optical observations of flux penetration.

The $c$-axis-oriented YBCO thin films were produced at Siemens Laboratories, Erlangen by a laser-ablation technique with a film thickness of 300 nm.[16] All thin films

 ©1995 The American Physical Society

were patterned chemically to be used for four-terminal resistivity measurements.

### B. Faraday effect

To visualize the magnetic field distribution of a superconductor we use the magneto-optical Faraday effect, i.e., the rotation of the polarization plane of linearly polarized light which passes a magneto-optically active layer exposed to the magnetic field of the underlying superconductor. Since the rotation angle depends on the magnetic field, we are able to visualize flux distributions as optical contrasts in a polarization microscope.

For the experiments presented in this paper, EuSe thin films were used as magneto-optical indicators. The EuSe thin films were deposited by electron-beam evaporation directly onto the sample surface, which was coated before with an aluminum layer of about 200 nm thickness in order to enhance its reflectivity.[11] This technique allows flux distributions to be observed directly with a spatial resolution of about 1 $\mu$m in a temperature range of 5 K $\leq T \leq$ 20 K. The lower-temperature limit is given by the cryostat; the upper limit is imposed by the strong temperature dependence of the Verdet constant of the europium chalcogenides.[8] However, flux distributions at temperatures $T >$ 20 K can be visualized indirectly by a special procedure during which the flux distribution obtained at a given temperature is observed after cooling the sample rapidly down to 5 K. This technique gives the correct flux patterns because during cooling the sample enters an undercritical state in which the flux distribution does not change.[14] The calibration technique of the measured light intensity in terms of the magnetic induction will be described in each particular case below.

## III. MODIFIED BEAN MODEL WITH $H_{c1}$

To describe the occurrence of flux steps at the flux front and at the sample edges one has to take into account finite $H_{c1}$ in the Bean model. In general the nonequilibrium flux penetration can be calculated using the equilibrium induction $B_{eq}(H)$ of a superconductor in a magnetic field.[5,6] In order to stress the sharpness of the flux steps we use the following triangular approximation for the equilibrium induction $B_{eq}$:

$$B_{eq}(H) = \begin{cases} \mu_0 (H - m_{eq} H_{c1}) & \text{for } H > H_{c1}, \\ 0 & \text{for } H < H_{c1}; \end{cases} \quad (1)$$

see also Fig. 1 and Ref. 17. Here, $m_{eq}$ denotes the reversible magnetization normalized by $H_{c1}$, which can range from 0 to 1.

The Lorentz force density acting on vortices inside the superconductor is given by

$$\mathbf{f_L} = \mathbf{B} \times (\nabla \times \mathbf{H}), \quad (2)$$

whereas the original Bean model assumes $\mathbf{f_L} = (1/\mu_0)\,\mathbf{B} \times (\nabla \times \mathbf{B})$, which is valid only for $H_{c1} = 0$. In Eq. (2), $\mathbf{H} = H(B)\mathbf{B}/B$ is determined locally by the material law given in Eq. (1). The flux-line motion starts when $\mathbf{f_L}$ exceeds the pinning force density $\mathbf{f_p} = \mathbf{j_c} \times \mathbf{B}$ if flux-creep effects are neglected. To find a solution of Bean's equilibrium equation $\mathbf{f_L} = \mathbf{f_p}$, i.e., $\mathbf{j_c} = \nabla \times \mathbf{H}$, in general is extremely difficult even in the critical state where we have now not only a homogeneous critical current density in the whole sample as for $H_{c1} = 0$, but also surface currents caused by finite $H_{c1}$. To calculate the magnetic field distribution we have to consider the *total* current density $\mathbf{j} = (1/\mu_0)\nabla \times \mathbf{B}$.

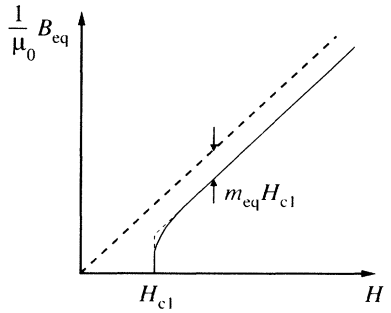


FIG. 1. Triangular approximation of the equilibrium magnetization curve of a type-II superconductor.

For an infinite slab of width $2a$ in the $x$ direction in a longitudinal magnetic field $\mathbf{H_a} \parallel z$ the equilibrium equation becomes one dimensional,

$$(\nabla \times \mathbf{H})_y = \frac{\partial H_z}{\partial x} = \left(\frac{\partial B_{eq}}{\partial H}\right)^{-1} \frac{\partial B_z}{\partial x} = j_c, \quad (3)$$

with the solution $H_z(x) = j_c x$ for $j_c =$ const. Note that this solution has a physical meaning only for $|H_a| > H_{c1}$. The flux-density profile then has precisely the shape of the equilibrium magnetization curve $B_z(x) = B_{eq}(j_c x)$. For $H_a < H_{c1}$ there is no flux penetration and the obtained flux step at the sample surface is caused by surface currents flowing in a $\lambda$ layer ($\lambda$ = London penetration depth), which fully screen the external magnetic field. In the triangular approximation, Eq. (1), when magnetic flux penetrates at $H_a > H_{c1}$, the maximum step of height $H_{c1}$ at the surface splits into two steps which are connected by Bean's critical gradient. The resulting profile is shown in Fig. 2(a). One step of height $m_{eq}H_{c1}$ remains at the sample surface $x = \pm a$ due to the difference between the external magnetic field $H_a$ and $B_{eq}$, which is caused by the screening currents reduced by $m_{eq}$. Another step occurs at the flux front $x = \pm x_0 = \pm(H_a - H_{c1})/j_c$. This flux step is due to surfacelike currents which flow inside the sample *in addition* to the critical current. For $x_0 \leq x \leq a$ and $H_{c1} < H_a < H^* = j_c a + H_{c1}$ the total current distribution is given by

$$j(x) = j_c + m_{eq} H_{c1} \delta(x - a) + (1 - m_{eq}) H_{c1} \delta(x - x_0)\,. \quad (4)$$

For $-a \leq x \leq -x_0$ we have $j(x) = -j(-x)$ and $j(x) = 0$ for $|x| < x_0$. In Eq. (4) Dirac's $\delta$ functions denote the surface currents at $x = a$ and the internal surfacelike currents at $x = x_0$. When $H_a$ exceeds the full penetration

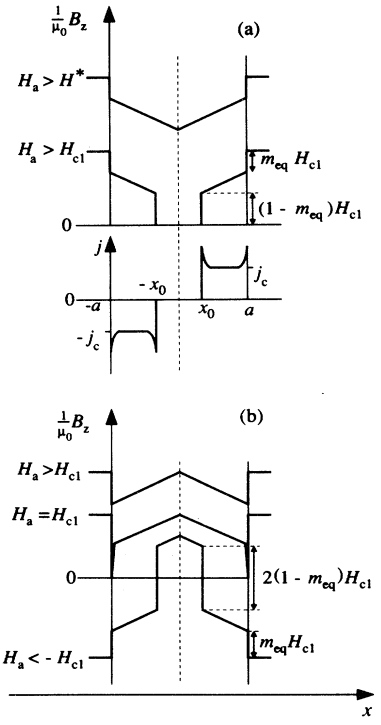


FIG. 2. Modified Bean model for a finite $H_{c1}$ in the triangular approximation. (a) Flux-density profiles in increasing external magnetic field. (b) Profiles in decreasing and reversing field after application of $H_a > H^*$.

field $H^*$ the steps at the two flux fronts annihilate and the third term in Eq. (4) disappears.

An illustrative access to find the shape of the profiles shown in Fig. 2 may be obtained by reproducing Fig. 1 on a slide. Then we put the slide in an empty $H(-a \leq x \leq a)$ diagram such that the abscissas of both diagrams coincide and the origin of Fig. 1 is located at the sample edge $x = a$. (For $x < 0$ all steps have to be carried out similarly but mirrored at the axis $x = 0$.) As the field is increased, Fig. 1 shifts towards $x = 0$ and the intersection of $B/\mu_0 = H$ (dashed line) with the line $x = a$ gives the value of the external field $H_a$. When the curve $(1/\mu_0)B_{eq}(H)$ meets the slab at $x = a$ we have $H_a = H_{c1}$ and the shape of the now penetrating flux-density profile is given by the curve $(1/\mu_0)B_{eq}(H)$. Another slide of Fig. 1, which is mirrored at the line $x = a$, is needed to demonstrate flux exit. In decreasing field this second slide is shifted towards $x = 0$ while the first slide is fixed (the penetrated flux is pinned); again the intersection of $B/\mu_0 = H$ (of the second slide) with $x = a$ marks the external field $H_a$. The shift stops when $H_a = H_{c1}$; i.e., $B_{eq}(H) = 0$ is located at $x = a$. A further reduction and reversing of $H_a$ does not cause any change of the flux distribution inside the slab until $H_a = -H_{c1}$. To illustrate penetration of reversed flux during further decrease of $H_a$ a third slides is needed, which is obtained from the second by rotating it by 180° around the point $x = a$ coinciding with $B_{eq}(H) = 0$. Now the second and the third slides have to be shifted together to obtain the shape of the flux profile, which is shown in Fig. 2(b). At $B_{eq}(H) = 0$ a step of height $2(1 - m_{eq})H_{c1}$ is observed; the value of $H_a$ is given now by the intersection of the dashed line $B/\mu_0 = H$ of the third slide with the sample edge $x = a$.

The main feature of the above considerations is the appearance of flux steps at the flux front and at the sample surface within the framework of Bean's critical-state model with finite $H_{c1}$. Both steps are due to currents which are concentrated in very narrow regions and *exceed* the critical current density. The flux step at the sample surface is due to the nucleation energy of new vortices in the Shubnikov phase. At the flux front there is a difference between the chemical potentials of the vortices in the Shubnikov and Meissner phases. This difference originates from the disappearing interaction between vortices at a distance $\lambda$.[5,6]

In our experiments we investigate flux distributions $B_z(\mathbf{r})$ at the surface of thin (lateral extension $\gg$ thickness $d$) HTSC's in a perpendicular external field. In this geometry logarithmic infinities of $B_z$ occur at the sample edges caused by demagnetization effects and the flux-density profiles exhibit a steep slope at the flux front.[18] Therefore it is very difficult to observe the flux steps during virgin magnetization in a perpendicular geometry. The observation is more reliable during reverse of the magnetization when we have flux steps of double height, which separate regions of flux with opposite polarity and are not overlapped by steep slopes of the profiles caused by the sample geometry.

## IV. OBSERVATION OF THE MAGNETIC STRUCTURE IN Bi2212

The optimal condition to visualize steps in the flux distribution is given in Bi2212 single crystals at $T = 20$ K where the critical current becomes comparable to the surface currents, $j_c \approx H_{c1}/d$. In Fig. 3(a) and 3(b) the flux penetration into a Bi2212 single crystal is shown for external magnetic fields, of $\mu_0 H_a = 107$ mT and $\mu_0 H_a = 171$ mT, respectively, in a crossed polarizer-analyzer setting. The external field is oriented perpendicular to the sample surface and hence parallel to its $c$ axis. The bright areas are the Shubnikov phase into which the flux lines have already penetrated, whereas the flux-free Meissner phase remains dark. Due to the demagnetizing fields, the flux penetrates mainly in the middle of each sample edge rather than from the corners.[19] The white arrows in Fig. 3(b) indicate the line along which the flux-density profiles in Fig. 4 were measured. Figures 3(c) and 3(d) show the flux distribution in the remanent state and at an applied reversed field of $\mu_0 H_a = -85$ mT, respectively. After switching off the external field the flux partly exits the crystal and the pinned vortices generate a stray field which allows flux of reversed polarity to enter at the sample edges; see Fig. 3(c) and Ref. 20. Here, we used an uncrossed polarizer-analyzer setting in order to obtain a linear relation between the measured light intensity $A$ and the magnetic induction $B_z$ near $B_z = 0$.[20]

Thus, the reversed magnetic flux at the sample edges appears darker than the trapped flux in the sample center. The Meissner phase is imaged at an arbitrary grey level. A detailed description of this procedure is given in Ref. 21. Note the expected very sharp transition between areas of trapped and newly entered flux, which is also seen in the profile in Fig. 4(b). Such sharp boundaries in flux distributions were also observed in YBCO at higher temperatures.[14]

The flux-density profiles which are depicted in Fig. 4 were calibrated from the initially measured light intensity $A$ in terms of $B$ by the following procedure: In the central dark zone, the Meissner phase, we have the intensity $A_0$ for $B_z = 0$. In the critical state the flux-density profile does not change its average slope but is only translated as a whole by the field change $\Delta H_a$. Thus the intersection of the profile with the line $B_z = 0$, i.e., the flux step, is shifted by a distance $\Delta x$ and $\partial B_z/\partial x = \mu_0(\Delta x/\Delta H_a)^{-1}$. Using the linearity of the $A$-$B_z$ characteristic near $B_z = 0$ one obtains $B_z(A)$ from

$$B_z(A) = \left(\frac{\partial B_z}{\partial x}\right)\left(\frac{\partial A}{\partial x}\right)^{-1}(A - A_0). \tag{5}$$

Note that this calibration works only near $B_z = 0$, as can be seen from Fig. 3(d) where the lowest flux density

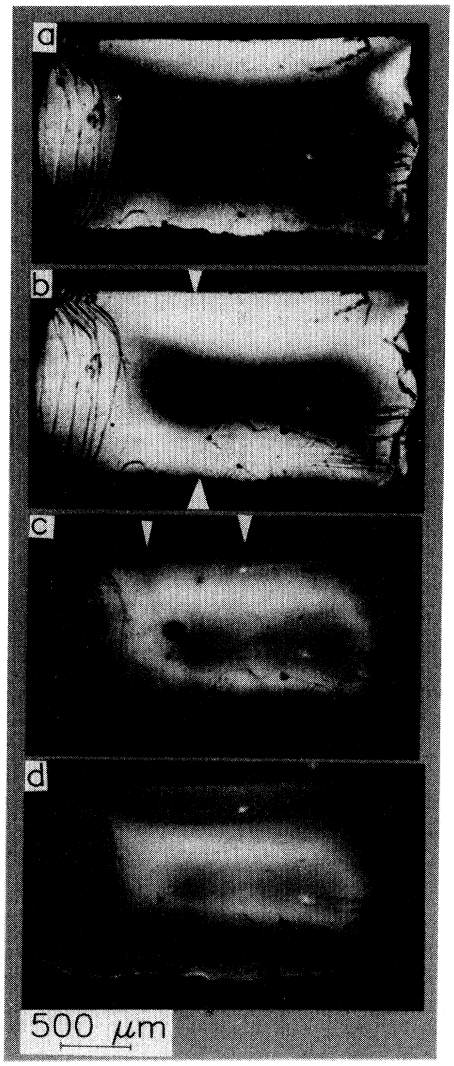


FIG. 3. Flux distributions in a Bi2212 crystal at $T = 20$ K. The external magnetic field is oriented perpendicular to the sample surface. (a) $\mu_0 H_a = 107$ mT; (b) 171 mT; the white arrows indicate the line along which the profiles in Fig. 4 were measured. (c) Remanent state of (b); the white arrows indicate the region which is shown in Fig. 5 with a higher magnification. (d) $-85$ mT. The reversed field is applied to the remanent state. The images (c) and (d) were obtained in an uncrossed polarizer-analyzer, setting thus that flux of reversed polarity is imaged darker than the trapped flux or the Meissner phase (see text).

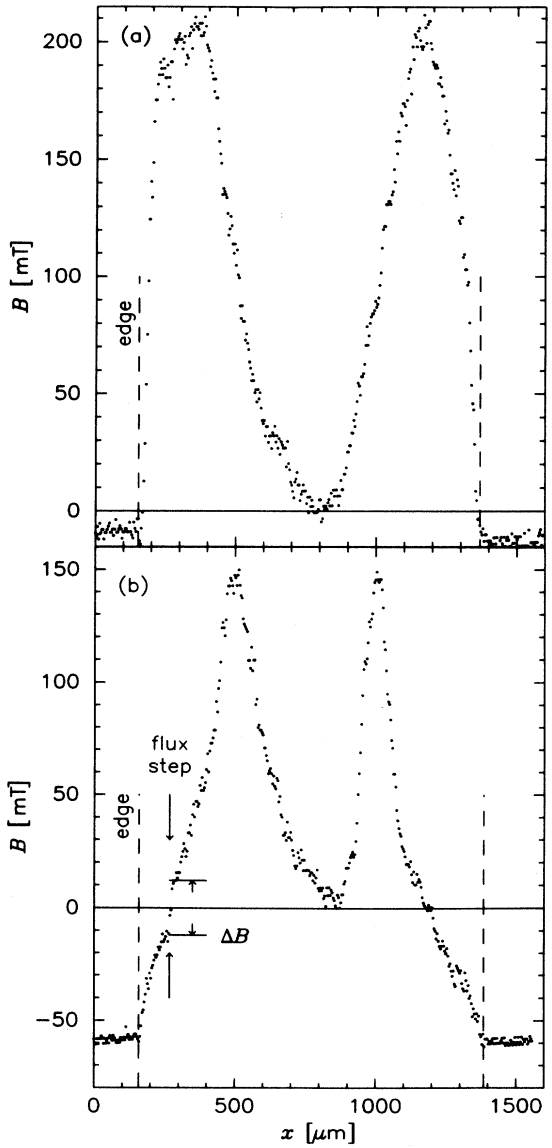


FIG. 4. Flux-density profiles measured along the line indicated by the white arrows in Fig. 3(b). (a) Penetrating flux, $\mu_0 H_a = 213$ mT, (b) remanent state after applying $\mu_0 H_a = 213$ mT.

is imaged bright, showing that the $A$-$B_z$ characteristic deviates from linearity and exhibits a minimum for larger $|B|$.

The flux-density profiles in Fig. 4 are similar to the ones obtained by the modified Bean model shown in Fig. 2. The penetrating profile [Fig. 4(a)] does not exhibit flux steps (see last paragraph in Sec. III) whereas in the remanent state [Fig. 4(b)] the predicted step of double height between pinned and newly entered reversed flux is well visible on the left side. On the right side of the profile the visibility of the flux step is reduced by the inhomogeneity of the sample surface. The step height is $\Delta B \approx 30$ mT, which is around $\mu_0 H_{c1}(\mathrm{Bi2212}) \approx 50$ mT for $H_a \parallel c$; see Ref. 22. For $m_{\mathrm{eq}} \approx 0.5$ (Ref. 17) it appears that good agreement between the experiment and the theoretical description in the previous section is obtained.

For detailed investigations the region marked by the white arrows in Fig. 3(c) was observed with higher magnification. The sequence of Fig. 5 shows the flux distribution after application of $\mu_0 H = 171$ mT at $T = 20$ K in (a) the remanent state and in applied fields of (b) $\mu_0 H_a = -11$ mT, (c) $-32$ mT, (d) $-64$ mT, (e) $-85$ mT, and (f) $-107$ mT. The shift of the flux step towards the sample center is clearly seen. The white arrows in Fig. 5(c) indicate the line along which the profile shown in Fig. 6 was measured. From this plot it is seen that the measured step height is not precisely $\Delta B = 2\mu_0(1 - m_{\mathrm{eq}})H_{c1} \approx \mu_0 H_{c1}$ in the linear slope induced by homogeneous $j_c$ with the corresponding shift (Fig. 2) but its shape is more similar to the bipolar field of a current string added to a linear profile. This can be clearly seen by subtracting the critical profile slope which is indicated by the dashed line in Fig. 6 as shown in the inset there. To explain this feature we have to take into account the particular flux distribution in a flat superconductor in a perpendicular magnetic field.

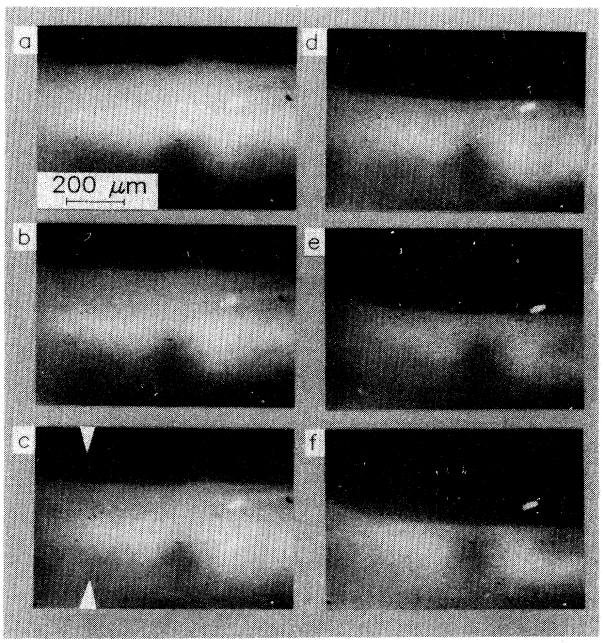


FIG. 5. Motion of the sharp front dividing the pinned and the newly entering reversed flux in increasing reversed field after application of $\mu_0 H_a = 171$ mT. (a) Remanent state, (b) $\mu_0 H_a = -11$ mT, (c) $-32$ mT, (d) $-64$ mT, (e) $-85$ mT, (f) $-107$ mT.

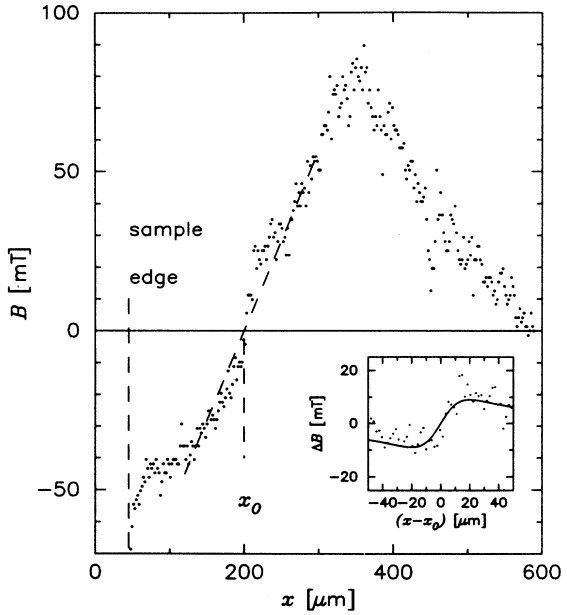


FIG. 6. Flux-density profile measured along the line indicated by the white arrows in Fig. 5(c). $x_0$ marks the position of the flux step between $B_z > 0$ and $B_z < 0$. The inset shows the region near $B_z = 0$ after subtraction of the averaged gradient determined by the homogeneous critical current density which is indicated by the inclined dashed line in the main graph and the theoretical curve of the field from a current string located at $x_0$ (solid line).

## V. CURRENT STRING IN A FLAT SUPERCONDUCTOR IN THE CRITICAL STATE

In a flat superconductor in a perpendicular magnetic field the Lorentz force $f_L$ is determined by the gradient $\partial B_x/\partial z$ rather than by the magneto-optically observed $\partial B_z/\partial x$; see Eq. (3) and Ref. 23. Here, the magnetic field lines strongly decline from the $z$ direction and in low magnetic fields they form closed loops *inside* the superconductor. Locally, the field lines which are closed around a central line $B_z = 0$ are similar to the situation of a transport current in an infinitely long superconducting cylinder, which was treated by Koppe.[24]

Following the description of Koppe, we consider a cylinder of radius $R$ carrying a critical transport current, which has a central core of radius $r_0 = H_{c1}/j_c$ where no current flows; see Fig. 7. However, the total current $I_{\mathrm{total}} = \pi R^2 j_c + I_0$ in the cylinder is higher than the critical current density integrated over the whole cylinder cross section by

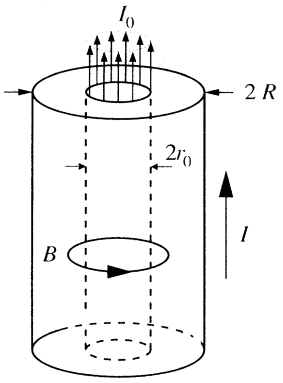


FIG. 7. Sketch of a transport current flowing in a type-II superconducting cylinder with a current string.

$$I_0 = \pi H_{c1}^2 / j_c \,. \tag{6}$$

In the triangular approximation [Eq. (1)] Koppe's solution of the current-density distribution takes the form

$$j = j_c - \frac{m_{eq} H_{c1}}{r} + m_{eq} H_{c1} \delta(r - R) + (1 - m_{eq}) H_{c1} \delta(r - r_0) \,. \tag{7}$$

For $m_{eq} = 0$ there is an excess current at the surface of the inner core of the value $2\pi r_0 H_{c1} = 2I_0$, and a compensating negative current of density $j_c$ inside the core, $\pi r_0^2 j_c = I_0$, in addition to the transport current density $j_c$ which would flow homogeneously in the whole cylinder volume for $H_{c1} = 0$. The inner core with the concentrated total extra current $I_0$ thus forms a feature within the superconductor which we call a current string. For $0 < m_{eq} \leq 1$ the current string is more widely distributed, but its total extra current $I_0$ remains the same. The current string is an intrinsic and universal macroscopic object of type-II superconductors.

In Fig. 8 the current distribution of our experimental situation is modeled for a slab in a perpendicular field in the critical state. Here, at the line $B_z = 0$ two current strings are added to the domains with the critical current density flowing in opposite directions. To estimate $I_0$ from our experimental data we subtract the averaged linear gradient (see Fig. 6) from the profile. The resulting curve which is depicted in the inset in Fig. 6 gives the field distribution $B_z^s(x)$ of the current string,

$$B_z^s(x) = \frac{\mu_0}{2\pi} \frac{I_0 x}{x^2 + (d/2)^2} \,. \tag{8}$$

For our sample with thickness $d = 40$ $\mu$m we obtain the best fit of Eq. (8) (solid line in the inset in Fig. 6) with the measured data points for $I_0 = 1.8$ A. Now, we can determine $j_c = 2.8 \times 10^5$ A/cm$^2$ from Eq. (6) with $H_{c1} = 50$ mT, which nicely agrees with $j_c = 3.5 \times 10^5$ A/cm$^2$ obtained by measuring the flux-penetration depth as it is described in Ref. 25.

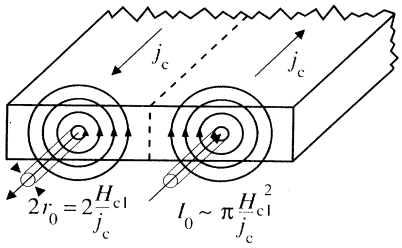


FIG. 8. Sketch of a flat superconductor in the critical state in perpendicular field with current strings. Two strings carrying the current $I_0$ flowing in opposite directions inside the characteristic domains of homogeneous critical current density $j_c$ are shown.

## VI. MAGNETIC FLUX DISTRIBUTION IN THE CRITICAL STATE OF A THIN FILM

From the previous considerations follows that the current string should cause an even larger effect in the flux distribution in thin films than in the plateletlike single crystals, because in samples with larger demagnetization factors the averaged gradient $\mu_0(\partial B_z/\partial x) \approx j_c d/a$ is

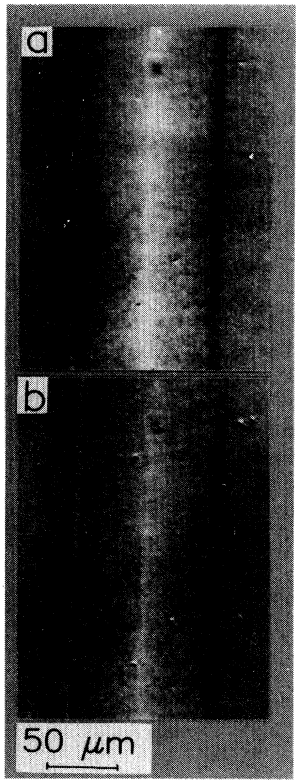


FIG. 9. Flux distribution in the remanent state of a thin YBCO strip of thickness $d = 300$ nm and half width $a = 50$ $\mu$m after applying $H_a > H^*$. (a) $T = 5$ K, (b) $T = 40$ K. The flux distributions were imaged in an uncrossed polarizer-analyzer setting in order to obtain a linear dependence of the light intensity from the magnetic field near $B_z = 0$. The dark lines mark the sample edges and do not contribute to the flux distribution. Here, the light is diffusely scattered due to surface damages during the patterning process.

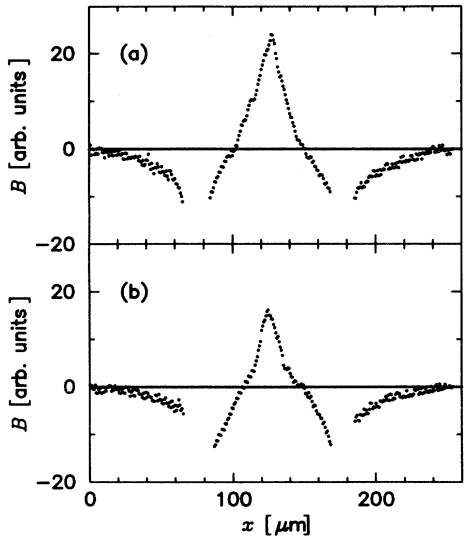


FIG. 10. Flux-density profiles measured across the strip shown in Fig. 9. (a) $T = 5$ K, (b) $T = 40$ K. The data points at the dark lines indicating sample edges were omitted.

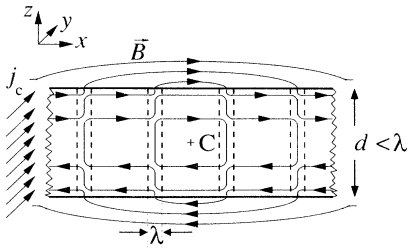


FIG. 11. Sketch of vortices and field lines in a thin ($d \ll \lambda$) type-II superconductor in a region near $B_z = 0$. The vortices with diameter $\lambda$ are shown by the vertical dashed lines. $C$ is the line where both $B_z$ and $B_x$ are zero. Note that the sketch is stretched in the $z$ direction for clarity. Interestingly, each field line can intersect many vortices.

smaller whereas the magnetic field step caused by the current string remains approximately $H_{c1}$. However, when $d/2 < r_0 = H_{c1}/j_c$, then the current string does not "fit" into the sample. To demonstrate this we observed flux distributions in a YBCO film ($d = 300$ nm, $a = 50$ $\mu$m) in the remanent state at $T = 5$ K and 40 K; see Figs. 9(a) and 9(b), respectively. In the whole temperature range where flux steps were observed in Bi2212 and YBCO (Ref. 14) single crystals, we cannot find any steps in the flux distribution or in the corresponding flux-density profiles (Fig. 10) of the thin film. Since with increasing temperature $j_c$ decreases more strongly than $H_{c1}$, $r_0$ is smallest at low temperatures; thus, at high temperatures the existence of current strings in thin films becomes more unlikely.

If the current string disappears because the vortices cannot form loops for $r_0 > d/2$, i.e., $H_{c1} > j_c d/2$, then the mode of vortex motion changes. Now, the surface current $J$ exerts a driving force on perpendicular vortices, $2J = j_c d$, *before* parallel vortices are able to penetrate since $J < H_{c1}$. This takes place also in thin films ($d \ll \lambda$) where the vortices are not curved because the surface currents flow homogeneously over the whole sample thickness.[26] The vortices remain straight whereas the field lines form loops as in the single crystals ($d \gg \lambda$) as shown in Fig. 11.

## VII. CONCLUSIONS

In conclusion, we have shown the existence of flux steps in Bi2212 single crystals by magneto-optics. To explain this feature we developed a model in the critical state with finite $H_{c1}$ which leads to the occurrence of current strings, i.e., additional supercurrents which are localized in a narrow string inside the homogeneous critical current flow at places where $B_z = 0$. The current string is proved to be a general macroscopic object in type-II superconductors. The movement of the current string inside the superconductor can be very complicated and may even lead to instabilities in the flux distribution, e.g., so-called macroturbulences which were observed in Ref. 27. The current string has a cylindric core of radius $r_0 = H_{c1}/j_c$ inside which no current flows. The additional supercurrent $I_0 = \pi H_{c1}^2/j_c$ is localized at the core surface if $m_{eq} = 0$. For $m_{eq} > 0$ the current $I_0$ gets smeared and flows outside the core. The radius $r_0$ is determined by the line tension (due to finite $H_{c1}$) of the vortices which form loops in regions near $B_z = 0$. The total current $I_0$ in the string increases with decreasing $j_c$ and thus the optimal conditions for the observation of flux steps are fulfilled in a temperature range where $j_c$ has decreased to $j_c \approx H_{c1}/d$ while $H_{c1}$ remains almost unchanged.

In thin films with thickness $d < 2r_0$, however, the current string cannot exist because the vortex loops collapse under their own tension for radii $r < r_0$ and the vortex motion is induced by the surface currents. For $d \ll \lambda \ll r_0$ the vortices always remain straight although the magnetic field lines can loop and the current string also cannot occur.

## ACKNOWLEDGMENTS

The authors wish to thank E. H. Brandt (Max-Planck-Institut) and G. D'Anna (Ecole Polytechnique de Lausanne) for fruitful discussions. We are grateful to B. Roas (Siemens AG, Erlangen, Germany) for the YBCO thin films. M.V.I. is grateful to the Alexander-von-Humboldt-Stiftung and to the Fond National Suisse de la Recherche Scientifique (FNPNR30 Grant No. 4030/32794) for financial support.

* Present address: Département de Physique, Ecole Polytechnique Fédérale de Lausanne, CH-1015 Lausanne, Switzerland. Permanent address: Institute of Solid State Physics, Russian Academy of Sciences, Chernogolovka, 142432 Moscow distr., Russian Federation.

[1] C. P. Bean, Phys. Rev. Lett. **8**, 250 (1962).
[2] S. Senoussi, J. Phys. (France) III **2**, 1041 (1992).
[3] *Concise Encyclopedia of Magnetic & Superconducting Materials*, edited by J. Evetts (Pergamon, Oxford, 1992).
[4] Y. B. Kim, C. F. Hempstead, and A. R. Strnad, Phys. Rev. **129**, 528 (1963).
[5] A. M. Campbell and J. E. Evetts, Adv. Phys. **21**, 199 (1972).
[6] H. Ullmaier, *Irreversible Properties of Type II Superconductors* (Springer, Berlin, 1975).
[7] V. M. Krasnov, V. A. Larkin, and V. V. Ryazanov, Physica (Amsterdam) C **174**, 440 (1991).
[8] R. P. Huebener, *Magnetic Flux Structures in Superconductors* (Springer, New York, 1979).
[9] H.-U. Habermeier and H. Kronmüller, Appl. Phys. **12**, 297 (1977).
[10] N. Moser, M. R. Koblischka, H. Kronmüller, B. Gegenheimer, and H. Theuss, Physica (Amsterdam) C **159**, 117 (1989).
[11] Th. Schuster, M. R. Koblischka, B. Ludescher, N. Moser, and H. Kronmüller, Cryogenics **31**, 811 (1991).
[12] M. V. Indenbom, N. N. Kolesnikov, M. P. Kulakov, I. G. Naumenko, V. I. Nikitenko, A. A. Polyanskii, N. F. Versinin, and V. K. Vlasko-Vlasov, Physica (Amsterdam) C **166**, 486 (1990).
[13] L. A. Dorosinskii, M. V. Indenbom, V. I. Nikitenko, Yu. A. Ossip'yan, A. A. Polyanskii, and V. K. Vlasko-Vlasov, Physica (Amsterdam) C **203**, 149 (1992).
[14] M. V. Indenbom, A. Forkl, H.-U. Habermeier, and H. Kronmüller, J. Alloys Compounds **195**, 499 (1993); M. V. Indenbom, Th. Schuster, M. R. Koblischka, A. Forkl, H. Kronmüller, L. A. Dorosinskii, V. K. Vlasko-Vlasov, A. A. Polyanskii, R. L. Prozorov, and V. I. Nikitenko, Physica (Amsterdam) C **209**, 259 (1993).
[15] T. W. Li, P. H. Kes, N. T. Hien, J. J. M. Franse, and A. A. Menovsky, J. Cryst. Growth **135**, 481 (1994).
[16] B. Roas, G. Endres, and L. Schultz, Appl. Phys. Lett. **53**, 373 (1988).
[17] L. Krusin-Elbaum, A. P. Malozemoff, D. C. Cronemeyer, F. Holtzberg, J. R. Clem, and Z. Hao, J. Appl. Phys. **67**, 4670 (1990); J. R. Clem and Z. Hao, Phys. Rev. B **48**, 13774 (1993).
[18] P. N. Mikheenko and Yu. E. Kuzovlev, Physica (Amsterdam) C **204**, 229 (1993); E. H. Brandt, M. V. Indenbom, and A. Forkl, Europhys. Lett. **22**, 735 (1993); E. H. Brandt and M. V. Indenbom, Phys. Rev. B **48**, 12 893 (1993); E. Zeldov, J. R. Clem, M. McElfresh, and M. Darwin, *ibid.* **49**, 9802 (1994).
[19] V. A. Rowe, R. P. Huebener, and R. T. Kampwirth, Phys. Status Solidi A **4**, 513 (1971); P. Brüll, D. Kirchgässner, and P. Leiderer, Physica (Amsterdam) C **182**, 339 (1991); Th. Schuster, M. Leghissa, M. R. Koblischka, H. Kuhn, M. Kraus, H. Kronmüller, and G. Saemann-Ischenko, *ibid.* **203**, 203 (1992); V. K. Vlasko-Vlasov, M. V. Indenbom, V. I. Nikitenko, A. A. Polyanskii, R. L. Prozorov, I. V. Grekhov, L. A. Delimova, I. A. Liniichuk, A. V. Antonov, and M. Yu. Gusev, Superconductivity **5**, 1637 (1992); Th. Schuster, M. V. Indenbom, M. R. Koblischka, H. Kuhn, and H. Kronmüller, Phys. Rev. B **49**, 3443 (1994); E. H. Brandt (unpublished).
[20] Th. Schuster, M. R. Koblischka, N. Moser, and H. Kronmüller, Physica (Amsterdam) C **179**, 269 (1991); Th. Schuster, M. R. Koblischka, B. Ludescher, and H. Kronmüller, J. Appl. Phys. **72**, 1478 (1992).
[21] Th. Schuster, M. R. Koblischka, H. Kuhn, B. Ludescher, M. Leghissa, M. Lippert, and H. Kronmüller, Physica (Amsterdam) C **196**, 373 (1992).
[22] N. Nakamura, G. D. Gu, and N. Koshizuka, Phys. Rev. Lett. **71**, 915 (1993).
[23] H. Theuss, A. Forkl, and H. Kronmüller, Physica (Amsterdam) C **190**, 345 (1992); D. Glatzer, A. Forkl, H. Theuss, H.-U. Habermeier, and H. Kronmüller, Phys. Status Solidi B **170**, 549 (1992).
[24] H. Koppe, Phys. Status Solidi **17**, 229 (1966).
[25] R. Knorpp, A. Forkl, H.-U. Habermeier, and H. Kronmüller, Physica (Amsterdam) C **230**, 128 (1994).
[26] E. H. Brandt, Phys. Rev. B **48**, 6699 (1993); E. H. Brandt and M. Indenbom, Physica B **194-196**, 1803 (1994).
[27] V. K. Vlasko-Vlasov, V. I. Nikitenko, A. A. Polyanskii, G. W. Crabtree, U. Welp, and B. W. Veal, Physica (Amsterdam) C **222**, 361 (1994).

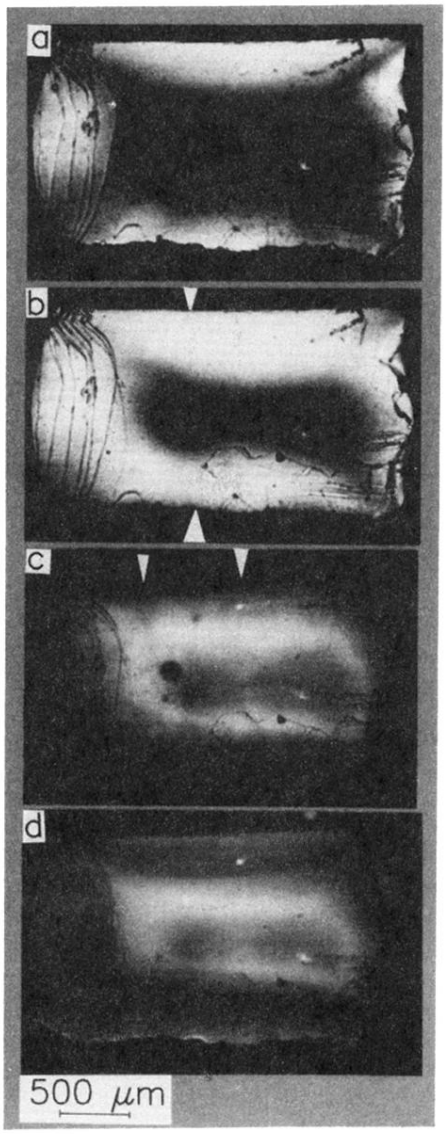


FIG. 3. Flux distributions in a Bi2212 crystal at $T = 20$ K. The external magnetic field is oriented perpendicular to the sample surface. (a) $\mu_0 H_a = 107$ mT; (b) 171 mT; the white arrows indicate the line along which the profiles in Fig. 4 were measured. (c) Remanent state of (b); the white arrows indicate the region which is shown in Fig. 5 with a higher magnification. (d) $-85$ mT. The reversed field is applied to the remanent state. The images (c) and (d) were obtained in an uncrossed polarizer-analyzer, setting thus that flux of reversed polarity is imaged darker than the trapped flux or the Meissner phase (see text).

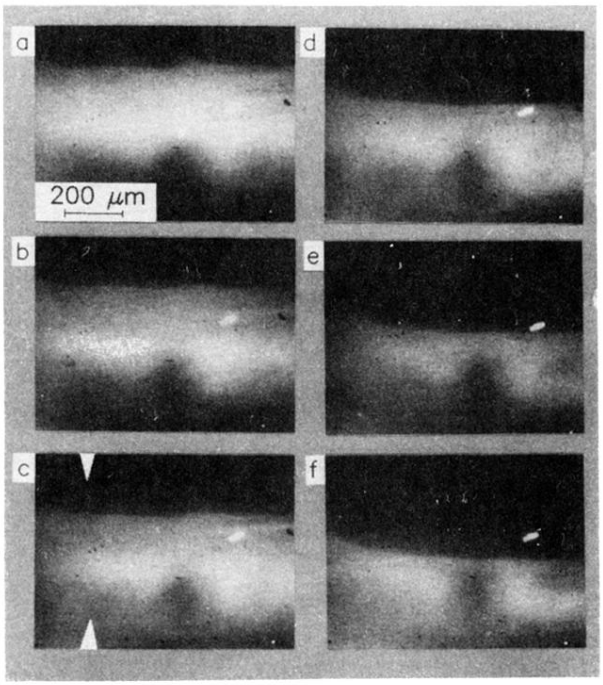


FIG. 5. Motion of the sharp front dividing the pinned and the newly entering reversed flux in increasing reversed field after application of $\mu_0 H_a = 171$ mT. (a) Remanent state, (b) $\mu_0 H_a = -11$ mT, (c) $-32$ mT, (d) $-64$ mT, (e) $-85$ mT, (f) $-107$ mT.

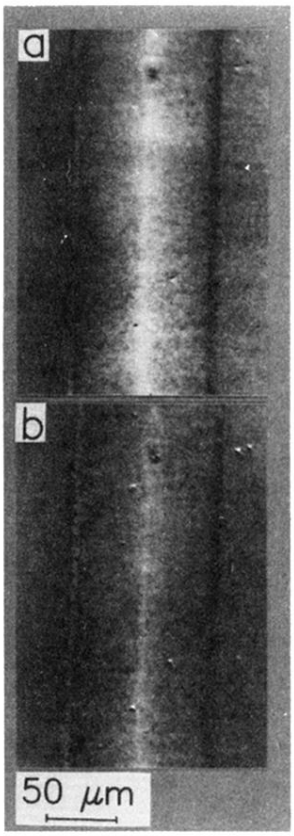


FIG. 9. Flux distribution in the remanent state of a thin YBCO strip of thickness $d = 300$ nm and half width $a = 50$ $\mu$m after applying $H_a > H^*$. (a) $T = 5$ K, (b) $T = 40$ K. The flux distributions were imaged in an uncrossed polarizer-analyzer setting in order to obtain a linear dependence of the light intensity from the magnetic field near $B_z = 0$. The dark lines mark the sample edges and do not contribute to the flux distribution. Here, the light is diffusely scattered due to surface damages during the patterning process.